A Comparison of an FDTD Thin-Slot Algorithm and Method of Moments for Modeling Slots Near Corners

K.-P. Ma, J. L. Drewniak, T. H. Hubing, and T. P. Van Doren
Electromagnetic Compatibility Laboratory
Department of Electrical Engineering
University of Missouri–Rolla
Rolla, Missouri 65401

Abstract

Subcellular FDTD algorithms for modeling thin slots in conductors have previously been developed. One algorithm that is based on a quasi-static approximation has been shown to agree well with experimental results for thin slots in planes. This FDTD thin-slot algorithm is compared herein with moment method results for thin slots near corners.

1 Introduction

The integrity of shielding enclosures is compromised by apertures and seams resulting from heatvents, cable penetration, and modular construction, among other possibilities. These perforations allow energy to be radiated to the external environment from interior electronic devices, or energy to be coupled from the exterior to interfere with interior components. An understanding of energy coupling mechanisms to and from the enclosure is essential to minimize potential radiation and susceptibility problems. Numerical methods have been applied to enclosure modeling for better understanding of these problems [1], [2]. The finite-difference time-domain (FDTD) method has previously been applied for modeling apertures in shielding enclosures as well as attached cables [1]. In these numerical methods, the aperture is typically modeled with widths on the order of the mesh dimension. In order to model a thin slot, or seam, the mesh dimension must be made small in the vicinity of the slot. This can consume significant computational resources. A subcellular FDTD method for modeling thin slots has previously been introduced by Gilbert and Holland [3]. Previous results show this simple and computationally efficient algorithm to agree well with experimental data, as well as with a more sophisticated integral equation based subcellular FDTD thin-slot algorithm [4].

The FDTD subcellular algorithm is compared with a mixed-potential integral equation formulation for slots near the corner of a 90^o bend in two dimensions. In the case of energy coupling through a thin slot with the axis parallel to the z-axis, only the TE_z case is important, since the TM_z case results in orders of magnitude less coupling [5]. A mixed-potential integral equation formulation is employed in order to incorporate the singularity in the charge distribution at the corner for the TE_z case [6]. Several cases of bend geometries are considered, with the slot located near the corner, and in the center of one of the strips. The FDTD results in general agree well with the moment method (MOM) for the three bend geometries considered when the slot is thin relative to the FDTD mesh dimension. However, when the slot becomes thick relative to the mesh dimension, the FDTD and MOM results begin to deviate considerably.

2 The Capacitive Thin-Slot Formalism

A subcellular capacitive thin slot formalism (C-TSF) based on an equivalent coplanar plate capacitance has previously been introduced by Gilbert and Holland [3]. The algorithm is developed to compute the electric field in the slot that is the field averaged over one mesh dimension. As a result, the electric-field component across the slot is significantly underestimated. However, immediately adjacent to the slot, the electric field computed with the C-TSF agrees very well with moment method results, experimental results, and another integral equation based FDTD subcellular method, [4], [7]. The C-TSF subcellular method has the advantage of being easily implemented and computationally efficient. Only the elec-

0-7803-3207-5/96/$5.00

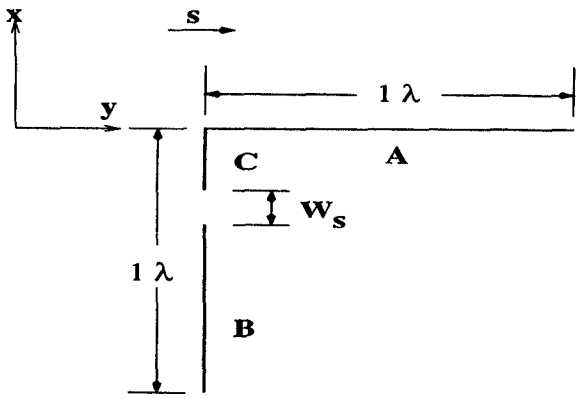

Figure 1: Geometry for a slot near a corner on a 2D finite bent strip

tric and magnetic field components in the slot require modification from the original FDTD time-marching scheme. The resulting algorithm is nearly identical to the usual FDTD equations with the exception that the slot capacitance is incorporated through an effective relative dielectric constant, and average field values are computed. The slot capacitance for parallel plates is given by an analytical form, and is related to an effective relative dielectric constant. A disadvantage of the method is that the slot length must coincide with an integral number of mesh dimensions. For larger mesh dimensions this leads to an inaccuracy in modeling the slot length. Practically though, where mesh dimensions on the order of $\frac{\lambda}{20}$ are necessary to achieve good results from FDTD computations, requiring the slot to be an integral number of mesh dimensions is not a serious limitation.

3 Comparison of C-TSF and MOM Modeling of Thin Slots Near Corners

The geometry employed for FDTD and MOM comparisons for modeling slots near corners is shown in Figure 1. The slot was located in two places along one arm of the bent conductor, in the center of one arm, and one cell from the edge. The present formulation of the C-TSF algorithm does not handle slots placed directly on corners, however, for practical purposes, a slot near the corner will result in much the same coupling effects to an enclosure. Square FDTD cells were employed with $\delta = \delta x = \delta y$. Mesh discretizations of $\delta = \frac{\lambda}{20}$, $\delta = \frac{\lambda}{40}$, and $\delta = \frac{\lambda}{80}$ were used. The bent-strip geometry was illuminated with an x-polarized electric-field incident plane wave with sinusoidal time variation. The FDTD time step was $t = \frac{0.00625}{f}$ s, where f was the operating frequency. A total-field/scattered-field formulation was used to implement the source [8]. Second-order Mur ABCs were employed.

The induced surface current density on the conducting strip was calculated from $\overline{\mathbf{J}}_s = \hat{\mathbf{n}} \times \left(\overline{\mathbf{H}}_{lit} - \overline{\mathbf{H}}_{shadow}\right)$, where $\hat{\mathbf{n}}$ is a unit normal vector directed into the lit region, and $\overline{\mathbf{H}}_{lit}$ and $\overline{\mathbf{H}}_{shadow}$ are the magnetic fields in the lit and shadow regions, respectively. For the 2D simulations being considered the surface current density is $J_x = H_{zi,jplate} - H_{zi,jplate-1}$,where only the $\hat{\mathbf{x}}$ component is given as an example. The magnetic-field components $H_{zi,jplate}$ and $H_{zi,jplate-1}$, are the magnetic-field components one half cell away from the strip in the shadow and lit regions, respectively.

A mixed potential-integral equation formulation was also employed for modeling the bent strip for comparison to the FDTD results [6]. In this formulation, a current basis function spans the bend, and charge basis functions end at either side of the corner in order to incorporate the singularity in the charge distribution at the corner. A Galerkin's procedure was employed with pulse basis and testing functions. In all cases, 100, 100, and 50 basis functions were used for Segments A, B, and C, respectively, as shown in Figure 1 [9]. Previous work by Glisson and Wilton has shown that this integral-equation formulation is sufficiently robust to accommodate a large jump in the segment length of the discretization.

FDTD C-TSF and MOM results are compared for a 1 $\lambda \times 1$ λ bent strip in Figures 2 and 3 ($B+C = 1$ λ, and $A = 1$ λ). In the figures, the bend is located at $\frac{s}{L} = 0$, and values of $\frac{s}{L} < 0$ denote the strip segment normal to the direction of the incident wave. In both cases, the FDTD mesh dimensions were $\delta = \frac{\lambda}{80}$, and the slot width was $w_s = 0.00125$ $\lambda = 0.1$ δ. The magnitude and phase of the current on the conducting bent strip with the slot in the center of the arm are shown in Figure 2. The FDTD subcellular and MOM results in general agree well for this case where the slot is located at a current maximum when the slot is not present. The magnitude differs most at the peaks, and there is a discrepancy in the phase around the bend. However, in the region of the slot the agreement is good. The computed current in the FDTD C-TSF case does not go to zero in the slot because this current is computed using values of the magnetic field on both sides of the strip that are displaced one-half cell from the strip. Since the currents on the bent strip agree well, the fields in the vicinity of the slot, as well as away from the strip will agree well also. Results of the current magnitude and phase for a slot located one FDTD cell off the corner are shown in Figure 3. Again the comparison between the FDTD subcellular and MOM results is good. In

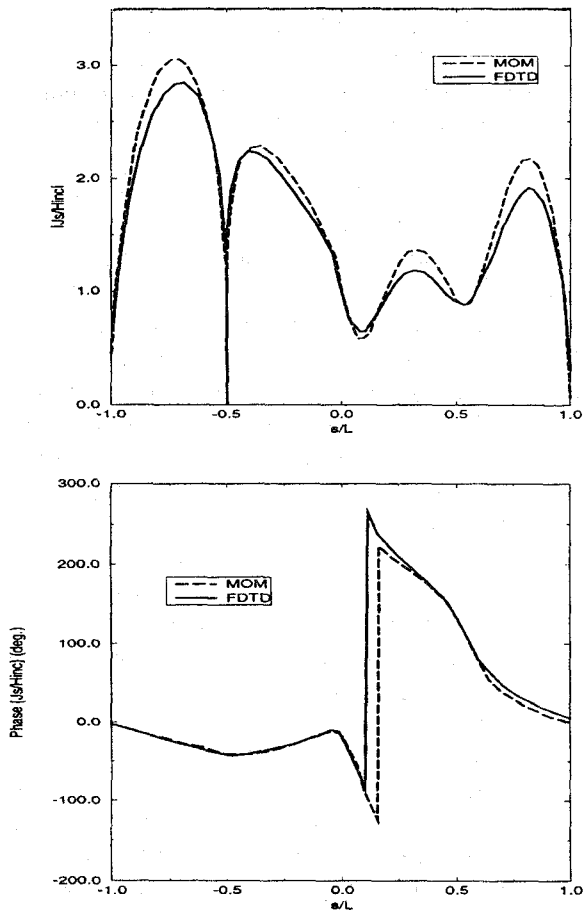

Figure 2: Comparisons of the magnitude and phase of the induced current on a 2D bent strip with a thin slot in the center of the $1\ \lambda \times 1\ \lambda$ arm for MOM and FDTD C-TSF.

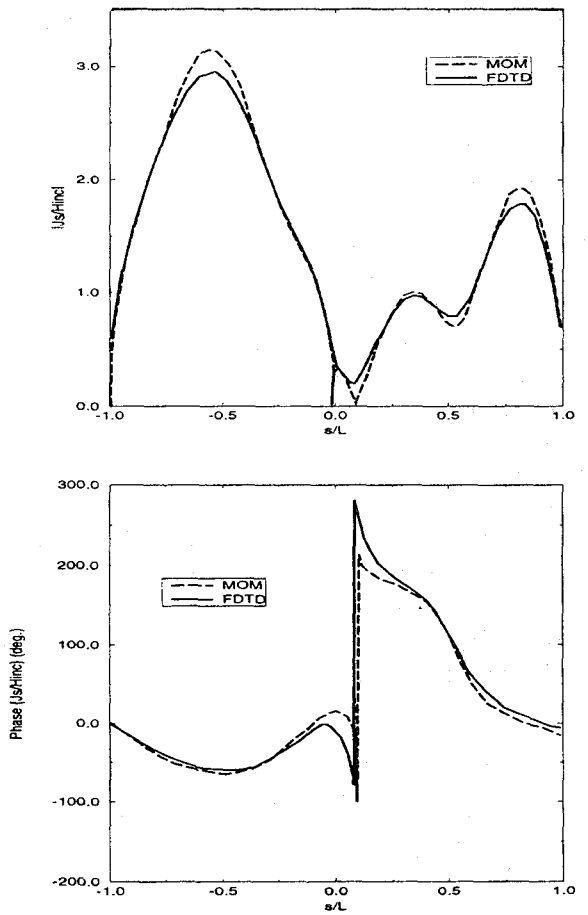

Figure 3: Comparisons of the magnitude and phase of the induced current on a 2D bent strip with a thin slot on the corner of the $1\ \lambda \times 1\ \lambda$ arm for MOM and FDTD C-TSF.

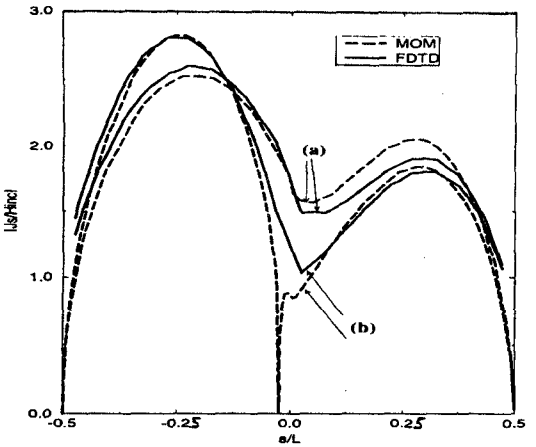

Figure 4: FDTD C-TSF and MOM comparisons of the magnitude of the induced current on a $\frac{\lambda}{2} \times \frac{\lambda}{2}$ 2D bent strip with (a) no slot and (b) a thin slot on the corner.

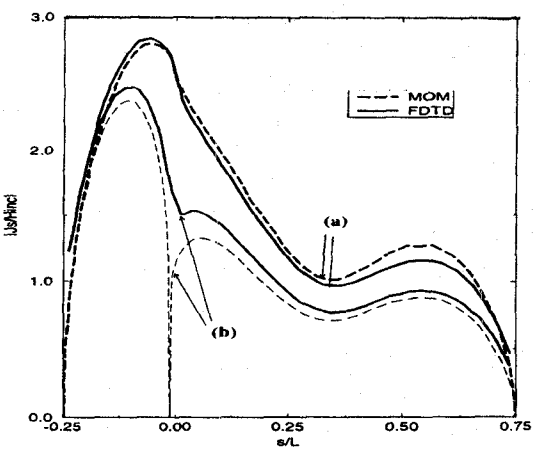

Figure 5: FDTD C-TSF and MOM comparisons of the magnitude of the induced current on a $\frac{\lambda}{4} \times \frac{3\lambda}{4}$ 2D bent strip with (a)no slot and (b) a thin slot on the corner.

this case the slot is located near a current minima, and has a small impact on the current distribution on the bent strip.

Other bent-strip geometries were also considered. In general it is not practical in FDTD modeling to discretize at $\delta = \frac{\lambda}{80}$. This level of detail throughout the computational domain consumes excessive memory. In the next case, mesh dimensions of $\delta = \frac{\lambda}{20}$ were employed. In addition, the slot width was changed to $w_s = 0.0002\ \lambda = 0.004\ \delta$. The magnitude of the current on a $\frac{\lambda}{2} \times \frac{\lambda}{2}$ bent strip is shown in Figure 4. Again the results agree well both without and with the thin slot. Larger slot dimensions were also studied with $\frac{w_s}{\delta} = 0.04$ and $\frac{w_s}{\delta} = 0.4$. The MOM and FDTD C-TSF results for $\frac{w_s}{\delta} = 0.04$ agreed well, however, when the slot width was on the order of the mesh dimension for $\frac{w_s}{\delta} = 0.4$, the agreement was poor.

The final case that was considered was for a $\frac{\lambda}{4} \times \frac{3\lambda}{4}$ bent strip. In this case the current on the strip without the slot is a maximum near the corner. Introducing the slot and forcing the current to go to zero on the front face of the bent strip significantly alters the current distribution. To allow at least ten FDTD cells to be employed for modeling the $\frac{\lambda}{4}$ bent strip, a mesh dimension of $\delta = \frac{\lambda}{40}$ was used. The slot width was changed as well so that $\frac{w_s}{\delta} = 0.004$, as in the previous case. The FDTD C-TSF and MOM results without and with a slot are shown in Figure 5. The results still agree well even when the thin slot is introduced near a current maximum on the strip. As in previous cases, when the slot width is on the order of the mesh dimensions $\frac{w_s}{\delta} = 0.4$, the agreement is poor.

4 Summary and Conclusions

A capacitive thin-slot formalism proposed by Gilbert and Holland for subcellular FDTD modeling has been implemented and compared with a mixed-potential integral equation formulation for modeling thin slots near corners. The case of a two dimensional bent strip was considered for several strip configurations. Available computational resources limited the comparisons to two dimensions. In general, the agreement was good for slot widths small relative to the mesh dimensions $\frac{w_s}{\delta} \leq 0.1$, however, for larger slot widths, the agreement deteriorates. In these cases, there is little advantage to a subcellular algorithm. Further, modeling a slot with a single FDTD cell will not adequately represent the field behavior in this region. In the case when a slot is on the order of a mesh dimension, a multi-grid or other suitable approach is necessary to adequately model the field behavior in the region of the slot.

References

[1] D. Hockanson, J. L. Drewniak, T. H. Hubing, and T. P. Vandoren, "Application of the finite-difference time-domain method to radiation from shielded enclosures," *IEEE Electromagnetic Compatibility Symposium Proceedings*, Chicago, IL, pp. 83-88, 1994.

[2] M. S. Tharf and G. I. Costache, "A hybrid finite element - analytical solutions for inhomogeneously filled shielding enclosures," *IEEE Trans. Electromagn. Compat.*, vol. 36, pp. 380-384, November 1994.

[3] J. Gilbert and R. Holland, "Implementation of the thin-slot formalism in the finite-difference EMP code THREDII," *IEEE Trans. Nuclear Sci.*, vol. NS-28, pp. 4269-4274, December 1981.

[4] K.-P. Ma, J. L. Drewniak, T. H. Hubing, and T. P. Van Doren, "A comparison of FDTD algorithms for subcellular modeling of slots in shielding enclosures," submitted to *IEEE Trans. Electromagn. Compat.*, May 1995.

[5] C. M. Butler, "A formulation of the finite-length narrow slot or strip equation, " *IEEE Trans. Antennas Propagat.*, vol. AP-30, pp. 1254-1257, November 1982.

[6] A. W. Glisson and D. R. Wilton, "Simple and efficient numerical methods for problems of electromagnetic radiation and scattering from surfaces," *IEEE Trans. Antennas Propagat.*, vol. AP-28, pp. 593-603, September 1980.

[7] C. D. Turner and L. D. Bacon, "Evaluation of a thin-slot formalism for finite-difference time-domain electromagnetic codes," *IEEE Trans. Electromagn. Compat.*, vol. 30, pp. 523-528, November 1988.

[8] A. Taflove, *Computational Electrodynamics.* Artech House; Boston, 1995.

[9] Kuang-Ping Ma, *Numerical Simulations for Thin Slot Penetration.* M.S. Thesis, University of Missouri-Rolla, 1995.